Research Article | Vol. 27, No. 10 | 13 May 2019 | OPTICS EXPRESS 13858
Optics EXPRESS

Topological bound modes in anti-PT-symmetric optical waveguide arrays

SHAOLIN KE,[1] DONG ZHAO,[2,3] JIANXUN LIU,[2] QINGJIE LIU,[2] QING LIAO,[1] BING WANG,[2,*] AND PEIXIANG LU[1,2,4]

[1]*Hubei Key Laboratory of Optical Information and Pattern Recognition, Wuhan Institute of Technology, Wuhan 430205, China*
[2]*School of Physics, Huazhong University of Science and Technology, Wuhan 430074, China*
[3]*School of Electronics Information and Engineering, Hubei University of Science and Technology, Xianning 437100, China*
[4]*lupeixiang@hust.edu.cn*
[*]*wangbing@hust.edu.cn*

Abstract: We investigate the topological bound modes in a binary optical waveguide array with anti-parity-time (PT) symmetry. The anti-PT-symmetric arrays are realized by incorporating additional waveguides to the bare arrays, such that the effective coupling coefficients are imaginary. The systems experience two kinds of phase transition, including global topological order transition and quantum phase transition. As a result, the system supports two kinds of robust bound modes, which are protected by the global topological order and the quantum phase, respectively. The study provides a promising approach to realizing robust light transport by utilizing mediating components.

1. Introduction

Topological photonics have attracted considerable attention as they provide additional degree of freedom to reveal new states of light [1–9]. They are also utilized for controlling light flows that is insensitive to disorder [1]. The simplest model to investigate topologically protected modes is the Su–Schrieffer–Heeger (SSH) model, which consists of binary arrays [10,11]. By tuning the intra- and inter- cell coupling, topological order of the array changes when a bandgap closes and then reopens. Topological protected modes appear at the gap of band structure when two structures with different topological orders are interfaced [1,11]. The SSH model is theoretically and experimentally reported in various optical systems, including metallic resonators [9], photonic superlattices [10], silicon waveguides [11], semiconductor micropillars [12], and plasmonic waveguides [13–17].

Studies of topological photonics have so far mostly dealt with Hermitian systems. Recently, a growing interest is paid to investigating topological properties of non-Hermitian systems with gain and loss, especially the Parity-Time (PT) -symmetric systems [18–27]. The PT symmetry is introduced to optics in 2008 for the first time [28], which requires the system Hamiltonian H obeys relation [PT, H] = 0. The system can possess real spectrum in the presence of gain and loss below PT-broken threshold [28–31]. The first experimental observation of PT symmetry is by utilizing two coupled semiconductor waveguides [29], where optical gain is provided though nonlinear two-wave mixing. Many fascinating phenomenon are reveled in PT-symmetric systems [31–35], such as double refraction [28], loss induced transparency [36], non-reciprocal propagation [29], and chiral mode switching [37–39]. Topological phase transition also emerges in PT-symmetric systems, which is closely related to the system degeneracy, known as exceptional point (EP) [19,21,23,40]. The topological bound modes with PT symmetry are firstly observed in coupled waveguide arrays [19], which are Hermitian-like and can be sustained with vanished gain and loss factor. Interestingly, PT-symmetric systems support unique robust bound mode with no Hermitian

#362178 https://doi.org/10.1364/OE.27.013858
Journal © 2019 Received 12 Mar 2019; accepted 21 Apr 2019; published 29 Apr 2019

Optics EXPRESS

counterparts. The bound modes appear at the interface between two arrays with same topological order but with distinct quantum phases [41–43].

Anti-PT-symmetric systems, which obey {PT, H} = 0 with the commutator replaced by the anticommutator, have also attracted much attention [44–49]. The original proposal of anti-PT symmetry is in [44], where the refractive index of the system satisfies $n(x) = -n^*(-x)$. The later studies demonstrate the discrete lattices with imaginary coupling can be anti-PT symmetric as well [45,47]. The imaginary coupling is realized in flying atoms [47], electric circuits [49], optical rings and waveguides by interacting the two bare states through a third state [45,46,48]. Many intriguing wave dynamics are found in anti-PT-symmetric systems. For example, flat broadband light transport and dispersion-induced dissipation are demonstrated in double waveguide coupler [45]. The chiral mode conversion by dynamically encircling an exceptional point (EP) is reported for symmetry-broken modes [48]. Actually, anti-PT symmetry belongs to a more fundamental symmetry called charge-conjugation symmetry [40,50,51], which is first proposed for superconductors and defined as {CT, H} = 0 with C being unitary operator [51]. The charge-conjugation symmetry is a general property of non-Hermitian systems consisting of two sublattices [50], which plays an important role in determining topological property of the system [40,50,52–54]. The study of asymmetric coupled systems indicates that the topological bound states can be generated via a degeneracy induced by charge-conjugation symmetry [40,52]. Moreover, the topological bound modes can be selectively pumped due to its special energy spectrum [50,54], which can be further utilized to enhance the lasing performance with improved single mode property, higher slope efficiencies, and robustness against perturbation [53,55–57].

In this work, we investigate the topological bound modes in anti-PT symmetric waveguide arrays with imaginary coupling. We show the imaginary coupling can be realized by incorporating assistant waveguides to the bare array and considering both gain and loss. The coupling strength can be further controlled by tuning the amount of gain and loss in respect waveguides. We show the topological phase transition in anti-PT-symmetric arrays is closely related to the imaginary part of band structure rather than its real part, which is different from the case in Hermitian and PT-symmetric systems. We also show the quantum phase transition can emerge by tuning the real part of refractive index, in contrast to PT-symmetric arrays in which the imaginary part of refractive index is altered. The robust bound states protected by global topological order and quantum phase are also discussed in detail.

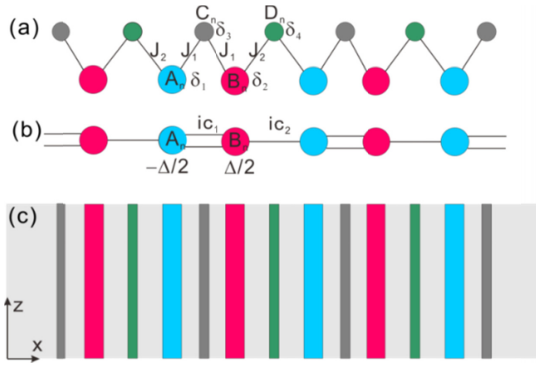

Fig. 1. Schematic of waveguide arrays with anti-PT symmetry. (a) The proposed sawtooth array to realize the effective imaginary coupling. The blue and red sites represent bare arrays and the gray and green are for assistant sites. (b) The equivalent array with imaginary coupling. (c) The geometry of proposed planar waveguide array with anti-PT symmetry.

2. Anti-PT symmetry and topological invariant

We start by investigating how to realize anti-PT-symmetric waveguide arrays with imaginary coupling. The non-Hermitian coupling emerges in coupled waveguides with gain or loss [58]

and also in open ring resonator with asymmetric scattering [59]. However, the imaginary part of coupling coefficient is small compared with its real part. Complex coupling is also realized by dynamically modulating refractive index along wave propagation direction [60,61]. However, it increased difficulties for experimental implementation. We follow another approach by incorporating assistant waveguides into the bare array to realize imaginary coupling [45,62,63]. The static on-site complex potentials simplify its practical implementation and the coupling strength can be tuned by the amount of gain and loss. As shown in Fig. 1(a), the proposed weekly coupled array have four waveguides in each unit cell, which are labeled as A, B, C, and D with C and D being the assistant waveguides. The corresponding effective detuning of propagation constants is denoted as δ_1, δ_2, δ_3, and δ_4. Only nearest coupling is considered. The coupling is represented by J_1 and J_2, which are assumed to be real and positive. The wave should evolve according to the coupled mode equation (CMT), which is given by

$$\begin{aligned} -i\frac{da_n}{dz} &= \delta_1 a_n + J_1 c_n + J_2 d_{n-1} \\ -i\frac{db_n}{dz} &= \delta_2 b_n + J_1 c_n + J_2 d_n \\ -i\frac{dc_n}{dz} &= \delta_3 c_n + J_1 (a_n + b_n) \\ -i\frac{dd_n}{dz} &= \delta_4 d_n + J_2 (a_{n+1} + b_n) \end{aligned} \tag{1}$$

where a_n, b_n, c_n, and d_n denote the field amplitudes in respect waveguide in nth unit cell. If the absolute value of detuning $|\delta_3|$ and $|\delta_4|$ are much larger than the coupling J_1 and J_2, the assistant waveguides C and D can be eliminated adiabatically [45], that is,

$$c_n = -\frac{J_1(a_n + b_n)}{\delta_3}, d_n = -\frac{J_2(a_{n+1} + b_n)}{\delta_4} \tag{2}$$

Substituting Eq. (2) into the first two terms of Eq. (1), the corresponding CMT reduces to

$$\begin{aligned} -i\frac{da_n}{dz} &= (\delta_1 - \frac{J_1^2}{\delta_3} - \frac{J_2^2}{\delta_4})a_n - \frac{J_1^2}{\delta_3} b_n - \frac{J_2^2}{\delta_4} b_{n-1} \\ -i\frac{db_n}{dz} &= -\frac{J_1^2}{\delta_3} a_n - \frac{J_2^2}{\delta_4} a_{n+1} + (\delta_2 - \frac{J_1^2}{\delta_3} - \frac{J_2^2}{\delta_4})b_n \end{aligned} \tag{3}$$

Therefore, after setting

$$\delta_1 = -i(c_1 + c_2) - \Delta/2, \delta_2 = -i(c_1 + c_2) + \Delta/2, \delta_3 = iJ_1^2/c_1, \delta_4 = iJ_2^2/c_2, \tag{4}$$

Equation (3) can be written as

$$\begin{aligned} -i\frac{da_n}{dz} &= -\frac{\Delta}{2} a_n + ic_1 b_n + ic_2 b_{n-1}, \\ -i\frac{db_n}{dz} &= ic_1 a_n + ic_2 a_{n+1} + \frac{\Delta}{2} b_n. \end{aligned} \tag{5}$$

The equivalent system described by Eq. (5) is depicted in Fig. 1(b). Each unit cell contains two waveguides A and B with effective detuning of propagation constants being ± Δ/2, respectively. The intra- and inter- coupling coefficients are ic_1 and ic_2, which are purely imaginary values. In order to realize the imaginary coupling, Eq. (4) indicates that the bare

Optics EXPRESS

arrays should be with gain and the assistant waveguides are with loss. Moreover, the amount of loss significantly exceeds the amount of gain, that is, $|\delta_3|$, $|\delta_4| \gg |\delta_1|$, $|\delta_2|$. As the adiabatic elimination requires $|\delta_3|$, $|\delta_4| \gg J_1$, J_2, the bare coupling strength should also be much larger than effective imaginary coupling, that is, J_1, $J_2 \gg c_1$, c_2.

For periodic boundary, the Bloch theorem can be utilized and the system Hamiltonian is given by

$$H = \begin{pmatrix} -\Delta/2 & ic_1 + ic_2\exp(-i\varphi) \\ ic_1 + ic_2\exp(i\varphi) & \Delta/2 \end{pmatrix}. \tag{6}$$

The time-reversal operation T transforms a z-independent operator to its complex conjugate, while the parity operator P exchanges locations of the modes [45]. Thus, the system Hamiltonian fulfills the relation $(PT)H(PT)^{-1} = -H$, which implies the system is anti-PT-symmetric. The anti-PT symmetry can be also defined by Pauli matrix σ_i, which requires $\sigma_x H(\varphi)\sigma_x = -H^*(\varphi)$ [23]. Chiral symmetry is also important in determining topological properties of the system, which is defined by $\sigma_z H(\varphi)\sigma_z = -H(\varphi)$. The system possesses chiral symmetry only when the detuning is $\Delta = 0$. This ensures the Berry phase of individual band is quantized. The eigenvalues of Eq. (6) are solved to be

$$\lambda_\pm = \pm\sqrt{\Delta^2/4 - c_1^2 - c_2^2 - 2c_1c_2\cos\varphi}. \tag{7}$$

The corresponding right and left eigenvectors are figured out as

$$\begin{aligned} |\lambda_+\rangle &= \begin{pmatrix} \cos(\Delta_k/2)\exp(i\phi_k) \\ \sin(\Delta_k/2) \end{pmatrix}, |\lambda_-\rangle = \begin{pmatrix} -\sin(\Delta_k/2)\exp(i\phi_k) \\ \cos(\Delta_k/2) \end{pmatrix} \\ \langle\mu_+| &= \begin{pmatrix} \cos(\Delta_k/2)\exp(-i\phi_k) \\ \sin(\Delta_k/2) \end{pmatrix}^T, \langle\mu_-| = \begin{pmatrix} -\sin(\Delta_k/2)\exp(-i\phi_k) \\ \cos(\Delta_k/2) \end{pmatrix}^T \end{aligned} \tag{8}$$

where $\Delta_k = \arctan(-2i\rho_k/\Delta)$ and $\rho(\varphi) = c_1 + c_2\exp(-i\varphi) = \rho_k\exp(i\phi_k)$. The system has three different phases according to anti-PT symmetry. When $|c_1 - c_2| > \Delta/2$, the system is in anti-PT-symmetric phase and eigenvalues are purely imaginary across the Brillion zone. When $|c_1 - c_2| < \Delta/2$, the system is in mixed anti-PT-symmetric and broken phases and eigenvalues become complex-valued at the edge of Brillion zone. When $|c_1 + c_2| < \Delta/2$, the anti-PT symmetry is fully broken and the eigenvalues develop into purely real values in the entire Brillion zone.

We now investigate the topological invariant and show the topological transition arises in anti-PT-symmetric systems. In non-Hermitian systems, the Berry phase for individual band is defined by $\varphi_B^\pm = \oint_k i\langle\mu_\pm|d/dk|\lambda_\pm\rangle dk$ [41], where ± labels the upper and lower bands and k represents Bloch momentum. The integration is taken over the 1D Brillouin zone. Substituting Eq. (8) into the expression for $\varphi \pm B$, the Berry phase is derived as

$$\varphi_B^\pm = -\oint d\phi_k/2 \pm \oint\cos(\gamma_k)d\phi_k/2 \tag{9}$$

When the chiral symmetry holds, that is, $\Delta = 0$, the second term of Eq. (9) is vanished. $\varphi \pm B$ is quantized to be an integer multiple of π, which is $\varphi \pm_B = \pi$ for $c_1 < c_2$ and $\varphi \pm B = 0$ for $c_1 > c_2$. In this situation, the Berry phase of individual band can be still regarded as topological invariant and utilized to indicate the topological phase transition. However, as $\Delta \neq 0$, the second term is not vanished. The Berry phase of a given band is not quantized and becomes complex-valued. Interestingly, the global Berry phase $\varphi G_B = \varphi_B^- + \varphi_B^+$ [41–43], which is

calculated by adding the complex Berry phase in both bands, remains quantized. Here we utilize global Berry phase to reveal the topological nature of anti-PT-symmetric waveguide arrays, which accurately captures the topological transition point $c_1 = c_2$.

3. Bloch modes

The above theory is general for weekly coupled lattices. As coupled waveguides have been widely utilized to demonstrate optical analogues of semi-classical electron dynamics [60,64–66], we now consider planar InGaAsP waveguides to exam above theoretical analysis. The geometry of proposed waveguide arrays is shown in Fig. 1(c). The structure is periodic along x direction and light propagates along z axis. There are four waveguides in each unit cell, which relative permittivity is denoted as ε_A, ε_B, ε_C, and ε_D. The real part of permittivity of InGaAsP is $\varepsilon_0 = 12.25$. The waveguides are assumed to be suspended in air with $\varepsilon_{air} = 1$ for simplicity. The width of waveguides w and the interlayer spacing d_0 are supposed to be uniform, which are given as $w = 0.24$ μm and $d_0 = 0.5$ μm, respectively. The incident wavelength is fixed at $\lambda = 1.55$ μm. The parameters are chosen such that a single waveguide only supports one propagating mode under TM polarization. The waveguides are weakly coupled when the spacing between adjacent waveguides is much larger than the full width half maximum of their eigenmode. In this work, the spacing is $d = d_0 + w = 0.74$ μm and the mode width is 0.31 μm. Therefore, the proposed geometry is in the weak coupling regime. We now investigate the band structures and the field distributions of Bloch modes of anti-PT-symmetric waveguide arrays, which can be calculated by transfer matrix method (TMM) [67,70]. The propagation constant of a single waveguide is figured out as $\beta_0 = 7.76$ μm^{-1}. The simulation shows the complex propagation constant of the single waveguide is $k_z \approx \beta_0 + 0.713\Delta\varepsilon$ with $\Delta\varepsilon$ denoting the detuned complex permittivity. The bare coupling strength J_1 and J_2 can be extracted from a Hermitian double waveguide coupler, which is determined as $J_1 = J_2 = J_0 = 0.047$ μm^{-1}. Then, the effective imaginary coupling can be realized by adding certain amount of gain and loss in respect waveguides according to Eq. (4). For example, the detuning of propagation constants, effective intra- and inter-layer coupling strength in Figs. 2(a) and 2(b) are $\Delta/2 = 2 \times 10^{-3}$ μm^{-1}, $c_1 = 4 \times 10^{-3}$ μm^{-1} and $c_2 = 1 \times 10^{-3}$ μm^{-1}, respectively. Then, the detuning of permittivity in waveguides A, B, C, and D should be $\Delta\varepsilon_A = (-2.8-7i) \times 10^{-3}$, $\Delta\varepsilon_B = (2.8-7i) \times 10^{-3}$, $\Delta\varepsilon_C = 0.77i$, and $\Delta\varepsilon_D = 3.09i$, respectively. The effective coupling strength can be properly controlled by tuning the detuning of imaginary part of permittivity.

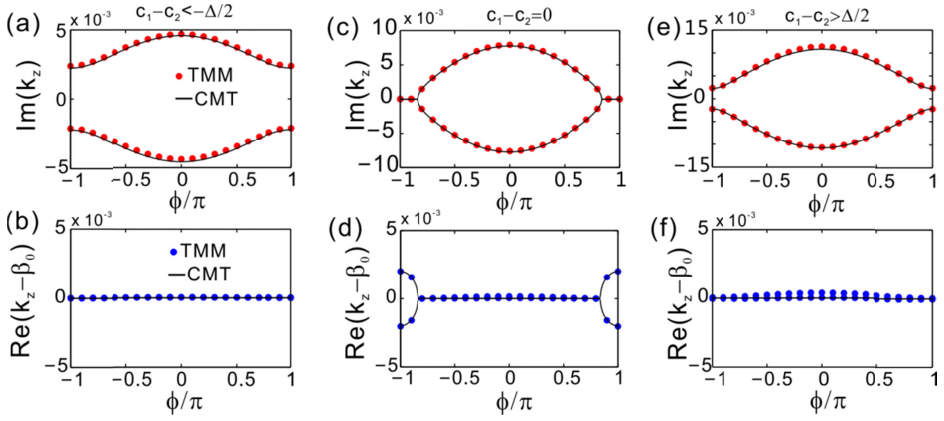

Fig. 2. The band structures of anti-PT-symmetric waveguide arrays for various coupling strength. (a), (c), and (e) The real part of band structure. (b), (d), and (f) The imaginary part of band structure. In all figures, the intra-layer coupling and the detuning of real part of propagation constant are fixed at $c_1 = 4 \times 10^{-3}$ μm^{-1} and $\Delta = 4 \times 10^{-3}$ μm^{-1}, respectively. The inter-layer coupling varies with (a) and (b) $c_2 = 1 \times 10^{-3}$ μm^{-1}, (c) and (d) $c_2 = 4 \times 10^{-3}$ μm^{-1}, (e) and (f) $c_2 = 7 \times 10^{-3}$ μm^{-1}.

Optics EXPRESS

Figure 2 plots the band structures in the first Brillouin zone for various inter-layer coupling, while the intra-layer coupling and detuning of real part of propagation constants remain unchanged. There are two bands in the system, representing two different kinds of Bloch modes. The lines stand for the results calculated by CMT according to Eq. (7) and the dots represent the simulations of TMM. In Figs. 2(a) and 2(b), the coupling strength fulfills the condition $c_1 - c_2 > \Delta/2$ and then the system should be in anti-PT-symmetric phase. In this phase, the imaginary part of band structure is gaped while the real part of the band structure is closed. As the coupling satisfies $|c_1 - c_2| < \Delta/2$, the imaginary part of band structure is closed. In Figs. 2(c) and 2(d), the coupling is $c_1 = c_2$. One can see the imaginary part of band structure closes at the EP near the edge of Brillion zone. As c_2 is further modified and fulfills $c_1 - c_2 < -\Delta/2$, as shown in Figs. 2(e) and 2(f), the imaginary part of band reopens and the real part remains closed. The simulation and the theoretical results coincide well with each other, which indicates the structure is surly in the weak coupling regime and the anti-PT-symmetric waveguide array is realized. The general topological band theory states that the topological phase of matter changes when a bandgap closes and then reopens when the system is further modified. In the Hermitian and PT-symmetric systems, the topological phase relates to the real part of band structure. Here in anti-PT-symmetric systems, we show the topological phase transition relates to the imaginary part of band structure as the real part of band structure is closed all the time. The system is topologic nontrivial as $c_1 < c_2$ and topological trivial as $c_1 > c_2$. Therefore, our study enriches the knowledge of topological transition. As the imaginary part of band structure is closed in the entire broken region ($|c_1 - c_2| < \Delta/2$), the band indices lose their meaning at a band crossing. Therefore, the topological invariant in the system is a property of the entire Hamiltonian, not individual bands [23].

Here we want to explain the role of Im(k_z) under propagation. The more amplified mode, that is, the mode have negative Im(k_z), would remain visible over a longer distance. Moreover, the amplified band structure can be extracted from the wave propagation for a broad Gaussian input beam. The imaginary part of band structure determines the amplification of total energy of Gaussian beam Im(k_z) = −Ln(E_{out}/E_{in})/2L, where E_{out} and E_{in} denote the output and input energy of Gaussian beam and L presents the total propagation distance. If a single waveguide is excited, the wave should evolve analogously to discrete diffraction with amplified energy subject to modified Bessel function [68].

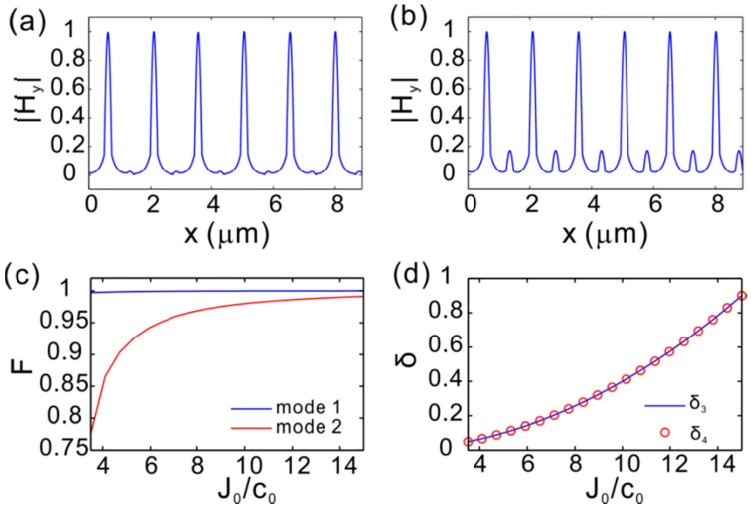

Fig. 3. (a) and (b) are the mode profiles of Bloch modes for $\varphi = 0$ in upper and lower bands, respectively. (c) The field fidelity as a function of coupling strength J_0. (d) The amount of loss added in assistant waveguides C and D for different coupling strength. In the calculation, $J_1 = J_2 = J_0$, $c_1 = c_2 = c_0 = 4 \times 10^{-3}$ μm^{-1}.

Optics EXPRESS

Figures 3(a) and 3(b) plot mode profiles ($|H_y|$) of Bloch modes at the center of Brillion zone corresponding to Fig. 2(c). Most of energy is confined at the bare waveguides A and B. The mode in upper band, as shown in Fig. 3(a), is almost perfect as the field in the assistant waveguide is almost vanished. However, the mode in lower band, as present in Fig. 3(b), is not ideal as a small amount of energy of is concentrated at the assistant waveguides C. In order to quantitatively compare the similarity of the eigenmode with that in ideal anti-PT-symmetric waveguide arrays, we define the field fidelity, which is given by

$$F = \sum_{m=\mathrm{A,B}} \left| \lambda_{+,m}^{*} \lambda_{m}^{'} \right|. \tag{10}$$

$|\lambda_{+,\mathrm{m}}\rangle$ and $|\lambda'_{+,\mathrm{m}}\rangle$ denote the normalized eigenvectors of ideal anti-PT-symmetric arrays and arrays with assistant waveguides, respectively. Considering the condition of adiabatic elimination and Eq. (4), the field fidelity should relate to J_1 and J_2, the bare coupling strength in arrays with assistant waveguides. Figure 3(c) plots the fidelity of two Bloch modes as a function of the ratio of bare coupling strength to effective imaginary coupling strength. The mode 1 at upper band is almost perfect as the field fidelity approximates to unity. The fidelity of mode 2 at lower band increases as the ratio of coupling strength increases and tends to unity as $J_0/c_0 \to \infty$. However, at the same time, the amount of loss added into the assistant waveguides is serious for large ratio. Figure 3(d) plots the detuning of imaginary part of propagation constants as a function of the ratio J_0/c_0. The detuning in assistant waveguide rapidly grows with the increase of coupling strength. It is difficult to realize huge amount of loss in experiment and it is also hard to maintain the real part of propagation constants. Therefore, the ratio of coupling strength should be carefully designed. For the mode shown in Figs. 3(a) and 3(b), the ratio of coupling strength is $J_0/c_0 = 11.75$. The field fidelity of two modes reaches as high as 0.9998 and 0.9856, which implies the arrays with assistant waveguides match well with the anti-PT-symmetric arrays.

4. Normal topological bound modes

In the above sections, we have discussed the band structure of periodic waveguide arrays and its topological invariant. One of most remarkably feature of topological photonics is that the interface between topologically inequivalent media necessarily hosts robust boundary modes. Now we study the topological bound modes in anti-PT-symmetric arrays.

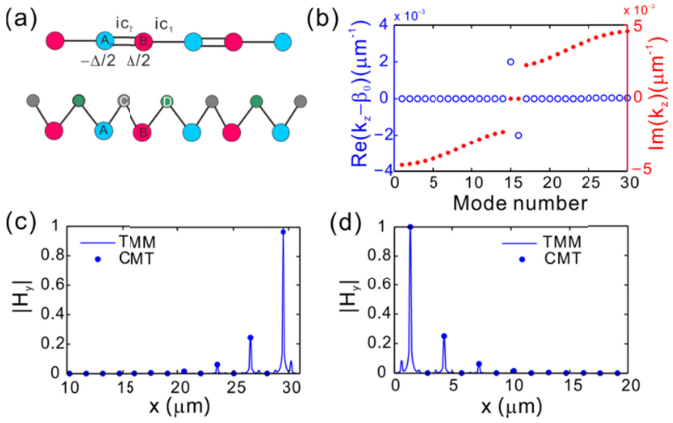

Fig. 4. Topological bound modes in finite waveguide arrays. (a) The geometry of finite lattice. (b) The propagation constants for all supermodes. (c) and (d) are the mode profiles for the topological edge modes. The effective coupling strength is $c_1 = 1 \times 10^{-3}$ μm^{-1} and $c_2 = 4 \times 10^{-3}$ μm^{-1}. The detuning of real propagation constant is $\Delta = 4 \times 10^{-3}$.

Optics EXPRESS

Figure 4(a) depicts the ideal finite waveguide arrays with imaginary coupling and the corresponding actual structure with assistant waveguides. The actual structure is terminated with assistant waveguides. The effective coupling strength is $c_1 = 1 \times 10^{-3}$ μm^{-1} and $c_2 = 4 \times 10^{-3}$ μm^{-1} and the detuning of propagation constants is $\Delta = 4 \times 10^{-3}$. As a result, the structure is topological nontrivial. The end of the structure can be regarded as the interface of two structures with different topological order, that is, the topological non-trivial waveguide array and the topological trivial air. Therefore, it must possess topological bound modes. The spectrum of propagation constants of the finite waveguide arrays is shown in Fig. 4(b). The number of bare waveguides is N = 30. One can see there is a pair of edge modes located at the gap of imaginary part of band. The imaginary part of propagation constants of two modes is equal while their real parts are different. The mode profiles of two edge modes are illustrated in Figs. 4(c) and 4(d). One mode is located at the right termination of the structure and the other is confined at the left. The lines represent the simulation results calculated by TMM and the dots are theoretical results for the ideal model. Despite of a small amount of energy confining to the assistant waveguides, the simulation agrees well with the theoretical indication. In Fig. 4(c), the field is mainly concentrated on waveguide A and waveguide B exhibits vanishing amplitude. In contrast, as plotted in Fig. 4(d), the energy is mainly distributed in waveguide B. The vanishing amplitudes at waveguide A or B is the result of topological protection on the edge mode as it prevents the edge mode from merging with bulk modes under a continuous deformation of the system's parameters.

On the other hand, as the inter-layer space d_0 is uniform between different waveguides, the system is topological trivial without considering gain and loss. The imaginary coupling strength is actually controlled by tuning the imaginary part of permittivity in assistant waveguides. Therefore, our results also indicate the topological phase transition is induced solely by gain and loss control, not the Hermitian factors [27]. Our model can also relate to previous study of SSH-like model with asymmetric coupling [21,40,52] by a basis change $(a_n', b_n')^T = (a_n, ib_n)^T$. After the basis change, the system Hamiltonian takes the form

$$H = \begin{pmatrix} -\Delta/2 & c_1 + c_2 \exp(-i\varphi) \\ -c_1 - c_2 \exp(i\varphi) & \Delta/2 \end{pmatrix}. \tag{11}$$

Both inter- and intra- coupling becomes asymmetric and the onsite potential is $-\Delta/2$ and $\Delta/2$. As $\Delta = 0$, the chiral symmetry is fulfilled, which retains the energy of topological mode to be zero, that is, $k_z = 0$. The nonvanished onsite potential Δ breaks chiral symmetry and the energy of topological mode is not remained at zero anymore, as shown in Fig. 4(b).

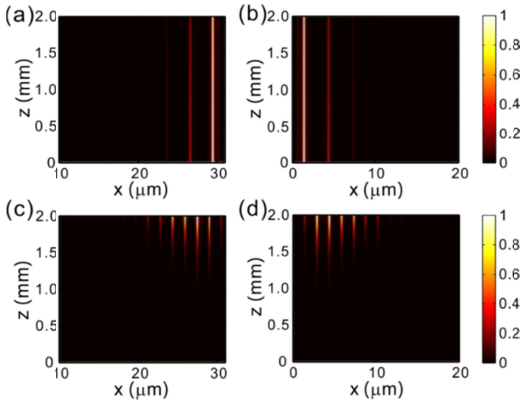

Fig. 5. Propagation of topological edge modes. In (a) and (b), the input fields are eigenmodes. (c) and (d) are for a single waveguide excitation from the right and left termination.

Optics EXPRESS

Figure 5 presents the propagation of two topological edge modes. The wave propagation is simulated using Rigorous coupled-wave analysis (RCWA) method [69]. In Fig. 5(a) and 5(b), the incident fields are the eigenmodes shown in Figs. 4(c) and 4(d). The fields are well confined at the ends of waveguide arrays during the propagation. The energy of two modes at different propagation distance z is almost neither decayed nor amplified. This agrees with the results shown in Fig. 4(b) as the imaginary part of propagation constants of two edge modes is zero. The situation is different when a single waveguide is excited. As shown in Figs. 5(c) and 5(d). The wave diffuses into the structure during the propagation. The reason can be understood. When wave is launched from the single waveguide, the bulk modes and the edge modes are excited simultaneously. As some bulk modes are more amplified than the edge modes, the bulk modes dominated after enough long propagation distance. In order to select the edge modes, one may pump the two waveguides at the structure termination as the edge modes are mostly confined at the termination waveguides.

5. Abnormal topological bound modes

In spite of the general topological phase transition, the previous study has shown that the PT-symmetric arrays also experience quantum phase transition. The quantum phase transition refers to an abrupt change of Berry phase of individual band [41–43]. Here we show the quantum phase transition emerges in the anti-PT-symmetric waveguide arrays as well.

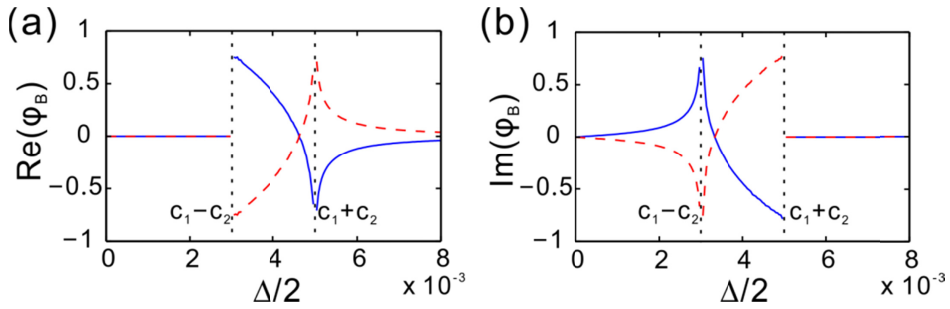

Fig. 6. The Berry phase as a function of detuning Δ. (a) Real part and (b) imaginary part of the Berry phase. The red and blue curves represent upper and lower bands, respectively. The effective coupling strength is $c_1 = 4 \times 10^{-3}$ μm^{-1} and $c_2 = 1 \times 10^{-3}$ μm^{-1}.

Figures 6(a) and 6(b) plot the complex Berry phase with increasing the detuning Δ as $c_1/c_2 > 1$. The results are numerically calculated by Eq. (9). In the limit $\Delta = 0$, the second term of Eq. (9) is vanished and the Berry phase is quantized. As Δ is not vanished, the Berry phase of individual band is not quantized and continuously varying by increasing the detuning Δ. The results can be divided into three phases. In phase I, that is, $c_1 - c_2 < \Delta/2$, the system is anti-PT-symmetric. The eigenvalues are purely imaginary and $\varphi_B^{\pm}$ are imaginary as well. In phase II, that is, $c_1 - c_2 < \Delta/2 < c_1 + c_2$, the eigenvalues become complex and the Berry phase is also complex. In phase III, that is, $\Delta/2 > c_1 + c_2$, the eigenvalues are real in the entire Brillion zone and the system is in fully anti-PT-broken phase. The Berry phase in this region is real. The three phases have distinct boundary as the Berry phase is not continuous. Any abrupt transition denotes the transition threshold where the system-associated quantum phase transits from one to another. Therefore, our system exhibits three different quantum phases. The unusual robust bound modes appear at the Phase I to III transition interface.

Optics EXPRESS

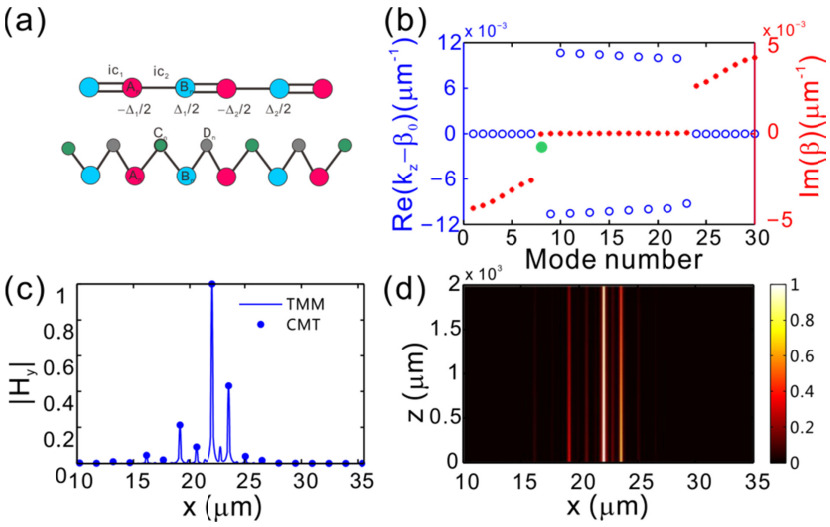

Fig. 7. Bound mode induced by quantum phase transition. (a) The proposed structures. (b) The spectrum of eigenmodes. The green dot denotes the robust bound modes. (c) The mode profiles of bound mode. The lines present the simulated results and the dots are the theoretical results calculated by the coupled mode theory. (d) Propagation of bound mode.

Figure 7(a) depicts the structures under consideration, where two semi-infinite waveguides with different quantum phases are interfaced. The coupling strength is set to be $c_1 > c_2$ such that the end of the structure will not support topological edge modes. The real part of propagation constants of two semi-arrays are different, which are denoted as Δ_1 and Δ_2. In the calculation, the parameters are chosen as $c_1 = 4 \times 10^{-3}$ μm^{-1}, $c_2 = 1 \times 10^{-3}$ μm^{-1}, $\Delta_1 = 0$, and $\Delta_2 = 22 \times 10^{-3}$ μm^{-1}, which satisfies the relation $\Delta_1/2 < |c_1 - c_2|$ and $\Delta_2/2 > |c_1 + c_2|$. Therefore, the two arrays are under the same topological order since global Berry phase are the same. However, their quantum phases are different. The left part is in the anti-PT-symmetric phase (phase I) and the right part is in fully anti-PT-broken phase (phase III). Figure 7(b) presents the propagation constants of all eigenmodes as the number of bare waveguides are set to be N = 30. There is an eigenmode located at the bandgap of the real spectrum, which is the robust mode generated by quantum phase transition. Figure 7(c) plots the mode profile of the bound mode, which energy is well concentrated at the interface. The simulated mode profile agrees well with the theoretical prediction, except that a small amount of energy resides at the assistant waveguides. Figure 8(d) shows the simulation results for the propagation of the bound mode. The energy is well confined to the center interface during the propagation.

The bound mode induced by the quantum phase transition is robust against topological disorder. To validate its robustness, we introduce a perturbation of coupling strength δ_c into the structure. Figure 8(a) depicts the ideal arrays as coupling near the interface is altered to be $c_1 - \delta_c$ and $c_2 + \delta_c$. The corresponding array with assistant waveguides is illustrated in Fig. 8(b). The permittivity of center five waveguides in the dotted box is changed while the geometric parameters remain unchanged. Figures 8(c) and 8(d) plot the mode profiles of the bound modes for different δ_c. The interface modes persist with field concentrated at the same waveguide, indicating its robustness against local topological perturbation. Remarkably, in Fig. 8(d), the local coupling strength is totally reversed ($c_1 < c_2$). In this situation, the bound modes can is not destroyed, showing large fault-tolerance. The lines and dots stand for the results of TMM and CMT, respectively. They are well accordant with each other.

Optics EXPRESS

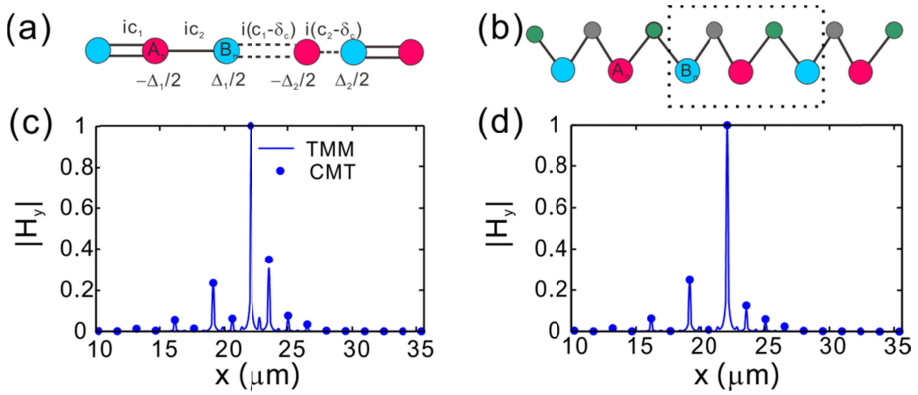

Fig. 8. Robustness of the bound mode against perturbation. (a) The proposed structures by tuning the local coupling strength at the interface. (b) The realistic structure with assistant waveguides. (c) and (d) are the mode profiles of bound modes as the perturbation of coupling strength is $\delta_c = 1 \times 10^{-3}$ μm^{-1} and 3×10^{-3} μm^{-1}, respectively.

6. Summary

In conclusion, we have studied a non-Hermitian extension of SSH model, that is, the topological bound modes in anti-PT-symmetric waveguide arrays with imaginary coupling. The imaginary coupling is realized by incorporating assistant waveguides to the two bare waveguides and considering both gain and loss. We show the system undergoes two different kinds of topological phase transition, including global topological order transition and quantum phase transition. As a result, the system supports two kinds of robust bound modes which are protected by the global topological order and the quantum phase, respectively. As the coupling strength can be flexibly controlled by tuning the amount of gain and loss, the topological phase transition can be controlled without tuning geometric parameters. In addition, the quantum phase transition can emerge by tuning the real part of refractive index, in contrast to PT-symmetric systems where the imaginary part of refractive index is modulated. The results enrich the study of topological photonics in anti-PT symmetric systems and may provide a way to realize robust light propagation by using mediating components.

Funding

National Natural Science Foundation of China (NSFC) (11804259, 11674117), Program for Distinguished Middle-aged and Young Innovative Research Team in Higher Education of Hubei, China (T201806), the Campus Science Foundation Research Project of Wuhan Institute of Technology (K201821).

References

1. L. Lu, J. D. Joannopoulos, and M. Soljačić, "Topological photonics," Nat. Photonics **8**(11), 821–829 (2014).
2. X. T. He, E. T. Liang, J. J. Yuan, H. Y. Qiu, X. D. Chen, F. L. Zhao, and J. W. Dong, "A silicon-on-insulator slab for topological valley transport," Nat. Commun. **10**(1), 872 (2019).
3. H. Deng, X. Chen, N. C. Panoiu, and F. Ye, "Topological surface plasmons in superlattices with changing sign of the average permittivity," Opt. Lett. **41**(18), 4281–4284 (2016).
4. H. Deng, Y. Chen, N. C. Panoiu, B. A. Malomed, and F. Ye, "Surface modes in plasmonic Bragg fibers with negative average permittivity," Opt. Express **26**(3), 2559–2568 (2018).
5. C. Shang, X. Chen, W. Luo, and F. Ye, "Quantum anomalous Hall-quantum spin Hall effect in optical superlattices," Opt. Lett. **43**(2), 275–278 (2018).
6. C. Liu, M. V. Gurudev Dutt, and D. Pekker, "Robust manipulation of light using topologically protected plasmonic modes," Opt. Express **26**(3), 2857–2872 (2018).
7. F. Wang, S. Ke, C. Qin, B. Wang, H. Long, K. Wang, and P. Lu, "Topological interface modes in graphene multilayer arrays," Opt. Laser Technol. **103**, 272–278 (2018).
8. P. Qiu, R. Liang, W. Qiu, H. Chen, J. Ren, Z. Lin, J. X. Wang, Q. Kan, and J. Q. Pan, "Topologically protected edge states in graphene plasmonic crystals," Opt. Express **25**(19), 22587–22594 (2017).

Optics EXPRESS

9. S. R. Pocock, X. Xiao, P. A. Huidobro, and V. Giannini, "Topological plasmonic chain with retardation and radiative effects," ACS Photonics **5**(6), 2271–2279 (2018).
10. N. Malkova, I. Hromada, X. Wang, G. Bryant, and Z. Chen, "Observation of optical Shockley-like surface states in photonic superlattices," Opt. Lett. **34**(11), 1633–1635 (2009).
11. A. Blanco-Redondo, I. Andonegui, M. J. Collins, G. Harari, Y. Lumer, M. C. Rechtsman, B. J. Eggleton, and M. Segev, "Topological optical waveguiding in silicon and the transition between topological and trivial defect states," Phys. Rev. Lett. **116**(16), 163901 (2016).
12. P. St-Jean, V. Goblot, E. Galopin, A. Lemaître, T. Ozawa, L. Le Gratiet, I. Sagnes, J. Bloch, and A. Amo, "Lasing in topological edge states of a one-dimensional lattice," Nat. Photonics **11**(10), 651–656 (2017).
13. Q. Cheng, Y. Pan, Q. Wang, T. Li, and S. Zhu, "Topologically protected interface mode in plasmonic waveguide arrays," Laser Photonics Rev. **9**(4), 392–398 (2015).
14. F. Bleckmann, Z. Cherpakova, S. Linden, and A. Alberti, "Spectral imaging of topological edge states in plasmonic waveguide arrays," Phys. Rev. B **96**(4), 045417 (2017).
15. L. Ge, L. Wang, M. Xiao, W. Wen, C. T. Chan, and D. Han, "Topological edge modes in multilayer graphene systems," Opt. Express **23**(17), 21585–21595 (2015).
16. Z. Wang, B. Wang, H. Long, K. Wang, and P. Lu, "Surface plasmonic lattice solitons in semi-infinite graphene sheet arrays," J. Lightwave Technol. **35**(14), 2960–2965 (2017).
17. D. Zhao, Z. Wang, H. Long, K. Wang, B. Wang, and P. Lu, "Optical bistability in defective photonic multilayers doped by graphene," Opt. Quantum Electron. **49**(4), 163 (2017).
18. R. El-Ganainy, K. G. Makris, M. Khajavikhan, Z. H. Musslimani, S. Rotter, and D. N. Christodoulides, "Non-Hermitian physics and PT symmetry," Nat. Phys. **14**(1), 11–19 (2018).
19. S. Weimann, M. Kremer, Y. Plotnik, Y. Lumer, S. Nolte, K. G. Makris, M. Segev, M. C. Rechtsman, and A. Szameit, "Topologically protected bound states in photonic parity-time-symmetric crystals," Nat. Mater. **16**(4), 433–438 (2017).
20. H. Schomerus, "Topologically protected midgap states in complex photonic lattices," Opt. Lett. **38**(11), 1912–1914 (2013).
21. S. Yao and Z. Wang, "Edge states and topological invariants of non-Hermitian systems," Phys. Rev. Lett. **121**(8), 086803 (2018).
22. S. Ke, B. Wang, H. Long, K. Wang, and P. Lu, "Topological edge modes in non-Hermitian plasmonic waveguide arrays," Opt. Express **25**(10), 11132–11143 (2017).
23. S. Lieu, "Topological phases in the non-Hermitian Su-Schrieffer-Heeger model," Phys. Rev. B **97**(4), 045106 (2018).
24. L. Jin, "Topological phases and edge states in a non-Hermitian trimerized optical lattice," Phys. Rev. A (Coll. Park) **96**(3), 032103 (2017).
25. B. Wu, J. Wang, M. Xiao, J. Xu, and Y. Chen, "Strong hybridization of edge and bulk states in dimerized PT-symmetric coupled waveguide chain," Opt. Express **25**(2), 1040–1049 (2017).
26. C. Yuce, "Edge states at the interface of non-Hermitian systems," Phys. Rev. A (Coll. Park) **97**(4), 042118 (2018).
27. K. Takata and M. Notomi, "Photonic topological insulating phase induced solely by gain and loss," Phys. Rev. Lett. **121**(21), 213902 (2018).
28. K. G. Makris, R. El-Ganainy, D. N. Christodoulides, and Z. H. Musslimani, "Beam dynamics in PT symmetric optical lattices," Phys. Rev. Lett. **100**(10), 103904 (2008).
29. C. E. Rüter, K. G. Makris, R. El-Ganainy, D. N. Christodoulides, M. Segev, and D. Kip, "Observation of parity–time symmetry in optics," Nat. Phys. **6**(3), 192–195 (2010).
30. Y. Li, X. Guo, C. Xu, J. Yang, X. Jiang, and M. Wang, "Coupled mode theory under the parity-time symmetry frame," J. Lightwave Technol. **31**(15), 2477–2481 (2013).
31. S. Ke, J. Liu, Q. Liu, D. Zhao, and W. Liu, "Strong absorption near exceptional points in plasmonic waveguide arrays," Opt. Quantum Electron. **50**(8), 318 (2018).
32. X. Lin, R. Li, F. Gao, E. Li, X. Zhang, B. Zhang, and H. Chen, "Loss induced amplification of graphene plasmons," Opt. Lett. **41**(4), 681–684 (2016).
33. S. Ke, J. Liu, Q. Liu, D. Zhao, and W. Liu, "Strong absorption near exceptional points in plasmonic waveguide arrays," Opt. Quantum Electron. **50**(8), 318 (2018).
34. A. Locatelli, A. D. Capobianco, M. Midrio, S. Boscolo, and C. De Angelis, "Graphene-assisted control of coupling between optical waveguides," Opt. Express **20**(27), 28479–28484 (2012).
35. J. Xu and Y. Chen, "General coupled mode theory in non-Hermitian waveguides," Opt. Express **23**(17), 22619–22627 (2015).
36. A. Guo, G. J. Salamo, D. Duchesne, R. Morandotti, M. Volatier-Ravat, V. Aimez, G. A. Siviloglou, and D. N. Christodoulides, "Observation of PT-symmetry breaking in complex optical potentials," Phys. Rev. Lett. **103**(9), 093902 (2009).
37. J. Doppler, A. A. Mailybaev, J. Böhm, U. Kuhl, A. Girschik, F. Libisch, T. J. Milburn, P. Rabl, N. Moiseyev, and S. Rotter, "Dynamically encircling an exceptional point for asymmetric mode switching," Nature **537**(7618), 76–79 (2016).
38. S. Ke, B. Wang, H. Long, K. Wang, and P. Lu, "Topological mode switching in a graphene doublet with exceptional points," Opt. Quantum Electron. **49**(6), 224 (2017).

Optics EXPRESS

39. S. Ke, B. Wang, C. Qin, H. Long, K. Wang, and P. Lu, "Exceptional points and asymmetric mode switching in plasmonic waveguides," J. Lightwave Technol. **34**(22), 5258–5262 (2016).
40. S. Malzard, C. Poli, and H. Schomerus, "Topologically protected defect states in open photonic systems with non-Hermitian charge-conjugation and Parity-Time symmetry," Phys. Rev. Lett. **115**(20), 200402 (2015).
41. S. Liang and G. Huang, "Topological invariance and global Berry phase in non-Hermitian systems," Phys. Rev. A **87**(1), 012118 (2013).
42. H. Zhao, S. Longhi, and L. Feng, "Robust light state by quantum phase transition in Non-Hermitian optical materials," Sci. Rep. **5**(1), 17022 (2015).
43. M. Pan, H. Zhao, P. Miao, S. Longhi, and L. Feng, "Photonic zero mode in a non-Hermitian photonic lattice," Nat. Commun. **9**(1), 1308 (2018).
44. L. Ge and H. E. Türeci, "Antisymmetric PT-photonic structures with balanced positive- and negative-index materials," Phys. Rev. A **88**(5), 053810 (2013).
45. F. Yang, Y. Liu, and L. You, "Anti-PT symmetry in dissipatively coupled optical systems," Phys. Rev. A (Coll. Park) **96**(5), 053845 (2017).
46. S. Ke, D. Zhao, Q. Liu, S. Wu, B. Wang, and P. Lu, "Optical imaginary directional couplers," J. Lightwave Technol. **36**(12), 2510–2516 (2018).
47. P. Peng, W. Cao, C. Shen, W. Qu, J. Wen, L. Jiang, and Y. Xiao, "Anti-parity–time symmetry with flying atoms," Nat. Phys. **12**(12), 1139–1145 (2016).
48. X. Zhang, T. Jiang, H. Sun, and C. T. Chan, "Dynamically encircling an exceptional point in anti-PT-symmetric systems: asymmetric mode switching for symmetry-broken states," arXiv:1806.07649.
49. Y. Choi, C. Hahn, J. W. Yoon, and S. H. Song, "Observation of an anti-PT-symmetric exceptional point and energy-difference conserving dynamics in electrical circuit resonators," Nat. Commun. **9**(1), 2182 (2018).
50. L. Ge, "Symmetry-protected zero-mode laser with a tunable spatial profile," Phys. Rev. A (Coll. Park) **95**(2), 023812 (2017).
51. D. I. Pikulin and Y. V. Nazarov, "Two types of topological transitions in finite Majorana wires," Phys. Rev. B Condens. Matter Mater. Phys. **87**(23), 235421 (2013).
52. F. K. Kunst, E. Edvardsson, J. C. Budich, and E. J. Bergholtz, "Biorthogonal bulk-boundary correspondence in non-Hermitian systems," Phys. Rev. Lett. **121**(2), 026808 (2018).
53. H. Zhao, P. Miao, M. H. Teimourpour, S. Malzard, R. El-Ganainy, H. Schomerus, and L. Feng, "Topological hybrid silicon microlasers," Nat. Commun. **9**(1), 981 (2018).
54. C. Poli, M. Bellec, U. Kuhl, F. Mortessagne, and H. Schomerus, "Selective enhancement of topologically induced interface states in a dielectric resonator chain," Nat. Commun. **6**(1), 6710 (2015).
55. M. Parto, S. Wittek, H. Hodaei, G. Harari, M. A. Bandres, J. Ren, M. C. Rechtsman, M. Segev, D. N. Christodoulides, and M. Khajavikhan, "Edge-mode lasing in 1D topological active arrays," Phys. Rev. Lett. **120**(11), 113901 (2018).
56. G. Harari, M. A. Bandres, Y. Lumer, M. C. Rechtsman, Y. D. Chong, M. Khajavikhan, D. N. Christodoulides, M. Segev, "Topological insulator laser: theory," Science **359**(6381), eaar4003 (2018).
57. M. A. Bandres, S. Wittek, G. Harari, M. Parto, J. Ren, M. Segev, D. N. Christodoulides, M. Khajavikhan, "Topological insulator laser: experiments," Science **359**(6381), eaar4005 (2018).
58. M. Golshani, S. Weimann, Kh. Jafari, M. K. Nezhad, A. Langari, A. R. Bahrampour, T. Eichelkraut, S. M. Mahdavi, and A. Szameit, "Impact of loss on the wave dynamics in photonic waveguide lattices," Phys. Rev. Lett. **113**(12), 123903 (2014).
59. J. Wiersig, "Structure of whispering-gallery modes in optical microdisks perturbed by nanoparticles," Phys. Rev. A **84**(6), 063828 (2011).
60. F. Wang, C. Qin, B. Wang, H. Long, K. Wang, and P. Lu, "Rabi oscillations of plasmonic supermodes in graphene multilayer arrays," IEEE J. Sel. Top. Quantum Electron. **23**(1), 125 (2017).
61. Q. Liu, S. Ke, and W. Liu, "Mode conversion and absorption in an optical waveguide under cascaded complex modulations," Opt. Quantum Electron. **50**(9), 356 (2018).
62. S. Longhi, "Non-Hermitian tight-binding network engineering," Phys. Rev. A (Coll. Park) **93**(2), 022102 (2016).
63. R. Keil, C. Poli, M. Heinrich, J. Arkinstall, G. Weihs, H. Schomerus, and A. Szameit, "Universal sign control of coupling in tight-binding lattices," Phys. Rev. Lett. **116**(21), 213901 (2016).
64. B. Xu, T. Li, and S. Zhu, "Simulation of massless Dirac dynamics in plasmonic waveguide arrays," Opt. Express **26**(10), 13416–13424 (2018).
65. J. Tan, Y. Zhou, M. He, Y. Chen, Q. Ke, J. Liang, X. Zhu, M. Li, and P. Lu, "Determination of the ionization time using attosecond photoelectron Interferometry," Phys. Rev. Lett. **121**(25), 253203 (2018).
66. C. Qin, B. Wang, H. Long, K. Wang, and P. Lu, "Nonreciprocal phase shift and mode modulation in dynamic graphene waveguides," J. Lightwave Technol. **34**(16), 3877–3883 (2016).
67. P. Yeh, "Optical waves in layered media," New York: Wiley, 1988.
68. S. Ke, Q. Liu, D. Zhao, and W. Liu, "Spectral discrete diffraction with non-Hermitian coupling," J. Opt. Soc. Am. B **35**(10), 2387–2393 (2018).
69. M. G. Moharam and T. K. Gaylord, "Rigorous coupled-wave analysis of planar-grating diffraction," J. Opt. Soc. Am. **71**(7), 811–818 (1981).
70. D. Zhao, D. Zhong, Y. Hu, S. Ken, W. Liu, "Imaginary modulation inducing giant spatial Goos-Hänchen shifts in one-dimensional defective photonic lattices," Opt. Quantum Electron. **51**(113), 1–11 (2019).